



IDENTIFICATION OF POTENTIAL ANTI-CANCER DRUG TARGET BY X-RAY CRYSTALLOGRAPHY, HIRSHFELD SURFACE, MOLECULAR DOCKING AND MOLECULAR DYNAMICS SIMULATION STUDIES

G. Dhanalakshmi¹, Anantha Krishnan Dhanabalan², Devadasan Velmurugan², Krishnaswamy Gunasekaran², VeluSaravanan³, A.K.Mohanakrishnan³, S. Aravindhan*¹

¹Department of Physics, Presidency College (Autonomous), University of Madras, Chennai, India

²Center of advanced studies in Crystallography and Biophysics, University of Madras, Guindy campus, Chennai, India

³Department of Organic Chemistry, University of Madras, Guindy Campus, Chennai, India

*Corresponding author: aravindhanpresidency@gmail.com

ABSTRACT

The mitogen-activated protein kinase (MAPK) p38 is a Ser/Thr kinase, originally isolated from lipopolysaccharide-stimulated monocytes. MAPK p38alpha represents a point of convergence for multiple signaling processes that are activated during inflammation, making it a key potential target for various diseases such as inflammatory diseases and cancer. In continuation of our studies on indole derivatives, two new compounds were synthesized and subjected to single crystal X-ray studies in order to investigate their molecular structure. Hirshfeld surface, docking analysis and Molecular Dynamics Simulations were also studied. Compound 1 and 2 crystallized in the monoclinic and orthorhombic crystal structure with P2₁/n and Pbc_a space groups respectively. The structures were solved by SHELXS and refined by SHELXL. In compound 1, the molecules are stabilized by a single weak C---H...O intermolecular interaction, four C---H...O intramolecular hydrogen bonds and an additional weak C---H...O intramolecular interaction. In compound 2, the molecules are stabilized only by weak C---H...O intra and intermolecular interactions, which generate S(6) ring motifs with the sulfone oxygen atoms. The intermolecular interactions of the compounds were analyzed using Hirshfeld surface analysis and two dimensional fingerprint plots, which confirms the XRD data. Induced fit docking method was used to find binding affinities parameters docking score, glide energy, favorable hydrogen bonding and hydrophobic interactions on the protein targets. The stability of the molecule in the presence of active site environment was found by using molecular dynamics simulation. All compounds shows better binding affinity similar to known existing cancer inhibitors.

Keywords: Crystal structure, Indole, Hirshfeld surface analysis, Molecular docking, Molecular Dynamics simulation.

1. INTRODUCTION

Indoles are heterocyclic compounds containing a pyrrole ring with a benzene ring fused to the a, b-position. Indole is an important heterocyclic system because it is the basis for the structure of amino acid tryptophan, and drugs like Indomethacin [1]. In the pharmaceutical industry indoles are used as intermediates for preparation of bioactive drugs [2]. Indole, being the important compound in nature, shows significant biological activity [3]. Indole derivatives are known to exhibit anti-depressant [4], anti-bacterial, anti-fungal [5], anti-inflammatory [6] anti-tumour [7] and physiological properties [8-9]. The Phenyl sulfonyl group of these Indole derivatives exhibit fungicidal, germicidal, and insecticidal activity [10-11]. They exhibit high aldose reductase inhibitory [12], and antimicrobial activities as well [13]. Indole derivatives are

also found to possess hypertensive, muscle relaxant [14] and antiviral [15] activities.

In the pharmaceutical industry, indoles are used as a popular component of fragrances and as a precursor such that, Indoles form the main classes of N-heterocycles. A survey on the literature of indoles showed more than 45000 results for indoles with biological activity [16]. Indoles are used in novel drugs with better and improved power [17]. Various synthetic methods have been used in the preparation of Indoles like Stoichiometric and catalytic reactions [18]. Researchers have found many methods for the preparation of indoles and numerous methods continue to be reported [19]. Indoles that are occurring naturally and synthetic indole containing molecules produced by various methods have important uses and potential as drugs with a wide range of

applications in many therapeutic classifications, like non-steroidic, anti-migrain, anti-depressant, anti-neoplastic and many others [20].

A Literature survey reveals that plants also contain the indole ring system [21]. Cytotoxic and anti-parasitic, properties were observed in Indole alkaloids extracted from plants [22]. Indole derivatives find applications as dyes, plastics, perfumes, as vitamin supplements and flavor enhancers [23]. Indoles, are used as anti-psychotic agents, anti-hypertensive drugs, anti-emetics, anti-depressants, anti-asthmatics, anti-virals, beta blockers, inhibitors of RNA polymerase-11, agonists for the cannabinoid receptor, non-nucleoside reverse, transcriptase inhibitors, opioid agonists, sexual dysfunctional agents, etc [24-28].

Cancer is one of the major life threatening diseases [29]. Chemotherapy treatment generally makes a patient suffer from serious adverse toxic effects. Hence, there is a urge for planning new chemotherapeutic agents targeting cancer cells with minimum side effects associated with the normal cells collateral damage [30]. Among the wide range of tested compounds as potential anticancer agents, indole derivatives have been described to exhibit outstanding antitumor activities [31].

In continuation of our studies on indole derivatives, two new compounds were synthesized and subjected to single crystal X-ray studies in order to investigate their molecular structure. Hirshfeld surface analysis, Docking studies and molecular simulations of the indole derivatives have been carried out to understand their intra and inter molecular interactions and the possibility of these compounds to act as an effective target.

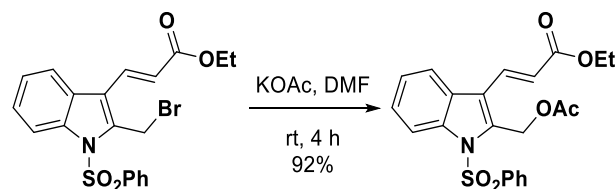
2. EXPERIMENTAL

2.1. Synthesis of compound1, C₁₈H₁₇NO₄S

A suspension of ethyl (*E*)-3-(2-(bromomethyl)-1-(phenylsulfonyl)-1*H*-indol-3-yl) acrylate (1.0 g, 2.23 mmol) and potassium acetate (0.43 g, 4.46 mmol) in DMF (10 mL) was stirred at room temperature for 8 h. After completion of the reaction (TLC), it was poured over crushed ice (100 g) containing Conc. HCl (5 mL). The precipitate obtained was filtered, washed with water (200 mL) and dried (CaCl₂).

The crude product upon crystallization from MeOH (5 mL) afforded ethyl (*E*)-3-(2-(acetoxymethyl)-1-(phenylsulfonyl)-1*H*-indol-3-yl)acrylate as a colorless solid (0.867 g, 91%); mp 114-116°C. ¹H-NMR (300 MHz, CDCl₃): δ 8.22 (d, *J* = 8.1 Hz, 1H), 7.95-7.82 (m, 4H), 7.57 (t, *J* = 7.05 Hz, 1H), 7.47-7.27 (m, 4H), 6.55 (d, *J* = 16.2 Hz, 1H), 5.61 (s, 2H), 4.29 (q, *J* = 6.9 Hz, 2H),

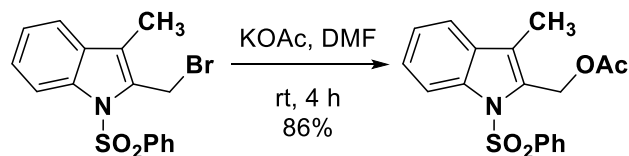
2.03 (s, 3H), 1.35 (t, *J* = 7.05 Hz, 3H) ppm. ¹³C-NMR (75 MHz, CDCl₃): δ 170.1, 166.7, 138.7, 136.9, 134.5, 134.2, 129.3, 126.8, 126.7, 126.4, 124.5, 121.8, 120.8, 120.5, 115.0, 60.8, 55.9, 20.7, 14.3 ppm.



Scheme 1: Synthesis of Ethyl (*E*)-3-(2-(acetoxymethyl)-1-(phenylsulfonyl)-1*H*-indol-3-yl) acrylate

2.2. Synthesis of compound2, C₁₇H₁₅N O₃S

To a solution of 2-(bromomethyl)-3-methyl-1-(phenylsulfonyl)-1*H*-indole (1.0 g, 2.74 mmol) in DMF (15 mL), potassium acetate (0.54 g, 5.49 mmol) was added. The reaction mixture was allowed to stir at room temperature for 4 h. After completion of the reaction (TLC), it was poured over crushed ice (100 g). Then, the solid obtained was filtered and crystallized from methanol to furnish the (3-methyl-1-(phenylsulfonyl)-1*H*-indol-2-yl)methyl acetate as a colorless solid (0.79 g, 84%); mp 82-84°C. The synthesis of compound 3 and compound 4 has already been reported [32].



Scheme 2: Synthesis of (Bromomethyl)-3-methyl-1-(phenylsulfonyl)-1*H*-indole

2.3. X-Ray Data collection, structure refinement and solution

X-ray diffraction intensity data were collected at room temperature (293K) on a Brukeraxs SMART APEXII single crystal X-ray diffractometer [33] equipped with graphite monochromatic MoK α ($\lambda=0.71073$ Å) radiation and a CCD detector.

The unit cell parameters were determined from 36 frames measured (0.5° phi-scan) from three different crystallographic zones using the method of difference vectors. The intensity data collection, frames integration, Lorentz and polarization corrections and decay

correction were carried out using SAINT-NT (version 7.06a) software [34].

An empirical absorption correction (multi-scan) was performed using the SADABS program [35]. A total of 42341 and 63123 reflections were collected for compound 1 and 2 respectively and among them 5788 and 2688 reflections were found to be unique for compound 1 and compound 2, respectively. The Crystal structures were solved by direct methods and then refined by the full matrix least-squares method using SHELXL [36] Figures were created using mercury and ORTEP-PLATON [37-39].

2.4. Hirshfeld surface analysis

Intermolecular contacts and their influence on the packing of the crystal structures were identified using Hirshfeld surface analysis [40-41]. The CIF files were used as input in the Crystal Explorer 17.5 [42] software package to draw the Hirshfeld surface mapped over d_{norm} . The combination of three colours red, blue and white in the factor d_{norm} has been used to analyze the intermolecular contacts. d_c and d^i are the two elements which denotes the distance of any surface point nearest to the interior atoms and the distance of the surface point nearest to the exterior atoms, respectively and also with the van der Waals (vdW) radii of the atom [43-44]. Hydrogen bonding contacts with negative d_{norm} value are indicated by the red colour circular spots. Longer contacts with positive d_{norm} value are indicated by the blue colour and the white colour indicates the intermolecular distances close to van der Waals radii with d_{norm} value equal to zero [45]. The shape of the electron density surface around the molecular interactions is indicated by the shape index. 2D fingerprint plots show the contribution of different type of intermolecular interactions of the molecule in the crystal [46-50].

2.5. Molecular docking

2.5.1. Protein preparation

The molecular docking study and modifications were carried out anti-cancer drug target proteins the Epidermal growth Factor receptor and p38alpha MAP Kinase PDB ID: 3POZ and 1W84 [51-52] which were retrieved from the protein data bank.

Missing hydrogen atoms were added and correct bond orders were assigned, and then formal charges and orientation of various groups were fixed. Following this, optimization of the amino acid, orientation of the hydroxyl and amide groups were carried out. All amino

acid flips were assigned and H-bonds were optimized. No hydrogen atoms were minimized until the average root mean square deviation reached the default value of 0.3 Å. Sitemap 2.3 was used to explore the binding site in the docking studies [53].

2.5.2. Ligand Preparation

All four synthesized indole compounds were constructed using the builder panel in Maestro. The compounds were taken for ligand preparation by the Ligprep 2.3 module [54] which performs addition of hydrogen, 2D to 3D conversion, realistic bond lengths and bond angles, low energy structure with correct chiralities, ionization states, tautomers, stereo chemistries and ring conformations.

2.5.3. Induced Fit Docking

Induced fit docking (IFD) is one of the main complicating factors in docking studies which predicts accurate ligand-binding modes and concomitant structural movements in the receptor using Glide and Prime modules. In IFD, when a ligand binds to the receptor, it undergoes a side chain or a backbone conformational change or both in many proteins.

These conformational changes allow the receptor to achieve better binding according to the shape and binding mode of the ligand. Here, the prepared protein was loaded in the workspace and the sitemap predicted active site was specified for IFD. The grid was calculated at about 20 Å to cover all the active site residues defined by the site map. The van der Waal's radii of the non-polar receptor and ligand atoms were scaled by a default factor of 0.50. IFD calculations were carried out for the anti-cancer target proteins. Following this, 20 conformational poses were calculated where the best conformational pose was selected based on the docking score, glide energy, hydrogen bonding and hydrophobic bonding interactions.

2.5.4. Molecular Dynamics Simulation

Based on the induced fit docking results, the best docking score of Compound 3 and Compound 4 and the cocrystal native compounds from the both target proteins and docked complexes were investigated to understand their stability of docked conformations of the ligands. A Molecular dynamics simulation was carried out using the Desmond program (version 5.0) with an inbuilt OPLS 2005 force field. The protein-ligand systems were set up for simulation using a predefined water model (TIP3P) as a solvent in an orthorhombic box of size 10 Å × 10 Å ×

10 Å with periodic boundary conditions. The neutral system for simulation was accomplished with the addition of 0.15 M NaCl using the system-built option. The system was relaxed using the predefined protocol consisting of the Steepest Descent and the limited-memory Broyden-Fletcher-Goldfarb Shanno algorithms in a hybrid manner. The system was simulated under the NPT ensemble. A constant temperature of 300K was maintained throughout the simulation using the Nose-Hoover thermostat algorithm and the Martyna-Tobias-Klein Barostat algorithm to maintain 1 atm of pressure with the isotropic coupling type. The final production run was carried out for 10 ns, and trajectory sampling was done at an interval of 1.0ps. Finally, the overall MD trajectories were analyzed and plotted using simulation interaction analysis. The Simulation trajectory was found to be stable and hence it confirms the appropriate docking of ligand and protein [53-58].

3. RESULTS AND DISCUSSION

3.1. Single crystal X-ray diffraction

The molecular structure of compound 1 is shown in Fig. 1. The compound crystallizes in monoclinic system with P21/n space group with two molecules per asymmetric unit. Similar structures were reported [59]. The three dimensional molecular structure of the compound was determined by X-ray crystallography using SHELXS and later refined by SHELXL. The R-factor value is slightly higher in compound 1 and this may be due to the small number of unique reflections. The mean plane of the sulfonyl bound phenyl ring [(C31-C36) in molecule A and (C13-C18) in molecule B] is almost orthogonal to the indole ring system [(N2/C19-C26) in molecule A, and (N1/C1-C8) in molecule B] making a dihedral angle of 80.3(2)° and 82.8(2)°, respectively. The mean plane of the acrylate ring [(C26-C29/O7-O8) in molecule A, (C8-C11/O3-O4) in molecule B] forms a dihedral angle of 72.9(3)° in molecule A and 89.02(8)° in molecule B with the indole ring system. The torsion angles for C27-O7-C28-C29 in molecule A and C9-O3-C10-C11 in molecule B are 175.0° and -175.5°, respectively. The sum of the bond angles at N2 is (359.12)° in molecule A and at N1 is (358.99)° in molecule B indicating sp² hybridization [60].

The molecular structure of compound 2, C₁₇H₁₅N O₃S is shown in Fig. 2. Literature survey shows that geometric parameters of compound 2 are in close agreement with those of similar structures [61]. The mean plane of the sulfonyl-bound phenyl ring (C1-C6) is

almost orthogonal to the mean plane of the indole ring system (N1/C7-C14), making a dihedral angle of 87.44(14)°. The C13-C14-C15-C16 torsion angle is 145°. The sum of the bond angles around N1 is 358.4°, indicating sp² hybridization.

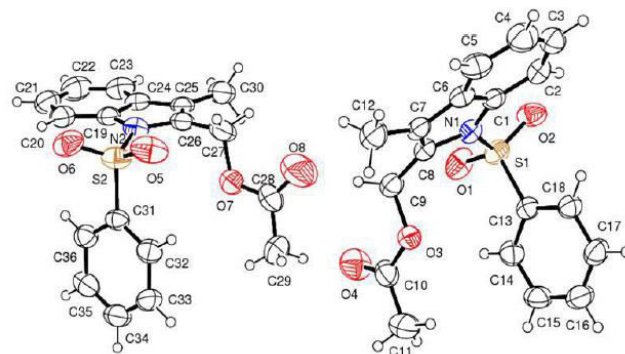


Fig.1: The ORTEP diagram of the compound 1 showing atom labeling with two molecules in the asymmetric unit. Displacement ellipsoids are drawn at the 40% probability level.

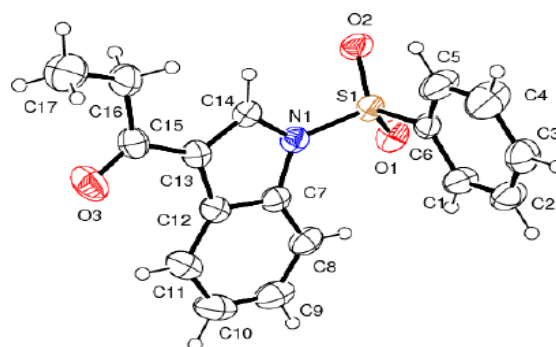


Fig. 2: The ORTEP diagram of compound 2 with the atom labeling. Displacement ellipsoids are drawn at the 40% probability level.

Atom S1 has a distorted tetrahedral configuration with angles O1-S1-O2 = 120.02° and N1-S1-C13 = 106.56 (19)° for compound 1 and O1-S1-O2 = 121.17 (13)° and N1-S1-C6 = 105.16 (11)° for compound 2, differing from the ideal tetrahedral values attributing to the Thorpe-Ingold effect [62]. As a result of the electron withdrawing character of the phenylsulfonyl group, in both compounds the N-C bond lengths [N1-C1 = 1.4215(2) Å and N1-C8 = 1.435(2) Å for compound 1 and N1-C14 = 1.387 (4) Å and N1-C7 = 1.418 (3) Å for compound 2] are longer than the mean value of 1.355 (14) Å [63].

In compound 1, the molecules are stabilized by a single weak C---H...O intermolecular interaction, four C---H...O intramolecular hydrogen bonds and an additional weak C---H...O intramolecular interaction (Table 5). In compound 2, the molecules are stabilized only by weak C---H...O intra and intermolecular interactions (Table 6), which generate S(6) ring motifs with the sulfone oxygen atoms.

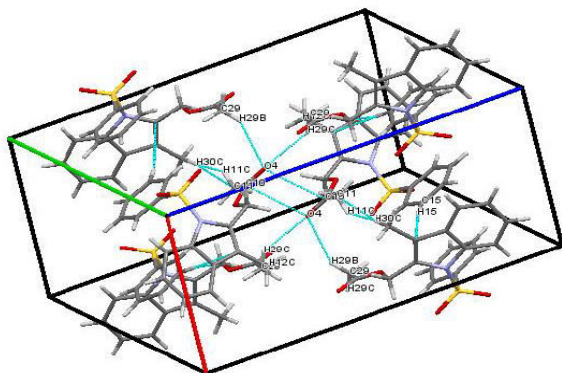


Fig. 3: The crystal packing of compound 1 viewed along the b- axis with dashed lines showing C---H---O hydrogen bonds and weak C---H---O intermolecular interactions.

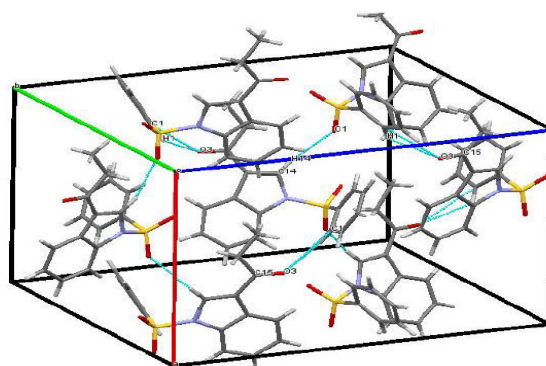


Fig. 4: The crystal packing of compound 2 viewed along the a- axis with dashed lines showing weak C---H...O intramolecular and intermolecular interactions.

In the crystal of compound 1, the molecules are linked via weak C29---H29...O4 intermolecular interactions and C2---H2...O2, C9---H9B...O1, C20---H20...O6 and C27---H27B...O5 intramolecular hydrogen bonds as well as an additional weak C29-H29C...O4 intramolecular interaction. In the crystal of compound 2, the molecules are linked via weak C1---H1...O3 and C14---H14...O1 intermolecular interactions and a weak C14---H14...O1 intramolecular interaction.

Table 1: Crystal data and structure refinement for compounds

Parameter	Compound 1	Compound 2
Formula weight	C ₁₈ H ₁₇ NO ₄ S 343.38	C ₁₇ H ₁₅ NO ₃ S 313.36
Temperature	296(2) K	296(2) K
Wavelength	0.71073 Å	0.71073 Å
Crystal system	Monoclinic	Orthorhombic
Space group	P2 ₁ /n	Pbca
Unit cell dimensions	a = 8.2174(4) Å	a = 11.3123(5) Å
	b = 23.1736(12) Å	b = 15.5403(7) Å
	c = 17.3446(9) Å	c = 17.4483(8) Å
Volume	3286.0(3) Å ³	3067.4(2) Å ³
Z	8	8
Density (calculated)	1.388 Mg/m ³	1.357 Mg/m ³
Absorption coefficient	0.219 mm ⁻¹	0.223 mm ⁻¹
F(000)	1440	1312
Crystal size	0.150 x 0.150 x 0.100 mm ³	0.150 x 0.150 x 0.100 mm ³
Theta range for data collection	2.117 to 24.994°	3.227 to 24.996°
Index ranges	-9 ≤ h ≤ 9,	-13 ≤ h ≤ 13,
	-27 ≤ k ≤ 27,	-18 ≤ k ≤ 18,
	-14 ≤ l ≤ 20	-20 ≤ l ≤ 20
Reflections collected	42341	63123
Independent reflections	5788 [R(int) = 0.0681]	2688 [R(int) = 0.0354]
Completeness to theta = 24.994°	100.00%	99.40%
Absorption correction	Semi-empirical from equivalents	Semi-empirical from equivalents

Max. and min. transmission	0.7452 and 0.6862	0.7460 and 0.7005
Refinement method	Full-matrix least-squares on F2	Full-matrix least-squares on F2
Data / restraints / parameters	5788 / 0 / 433	2688 / 0 / 201
Goodness-of-fit on F2	1.06	1.207
Final R indices [$I > 2\sigma(I)$]	R1 = 0.0621, wR2 = 0.1536	R1 = 0.0491, wR2 = 0.0995
R indices (all data)	R1 = 0.1314, wR2 = 0.2146	R1 = 0.0626, wR2 = 0.1141
Largest diff. peak and hole	0.677 and -0.433 e.Å ⁻³	0.261 and -0.310 e.Å ⁻³

Table 2: Selected Bond lengths [Å] for Compounds

Compound I		Compound II			
Bond	Bond length [Å]	Bond	Bond length [Å]	Bond	Bond length [Å]
C(1)-C(2)	1.392(6)	C(16)-C(17)	1.363(7)	C(1)-C(6)	1.376(4)
C(1)-C(6)	1.401(6)	C(17)-C(18)	1.381(6)	C(1)-C(2)	1.380(4)
C(1)-N(1)	1.421(5)	C(19)-C(20)	1.384(6)	C(2)-C(3)	1.357(4)
C(2)-C(3)	1.372(7)	C(19)-C(24)	1.402(6)	C(3)-C(4)	1.368(5)
C(3)-C(4)	1.385(7)	C(19)-N(2)	1.416(6)	C(4)-C(5)	1.382(5)
C(4)-C(5)	1.375(7)	C(20)-C(21)	1.378(7)	C(5)-C(6)	1.368(4)
C(5)-C(6)	1.387(6)	C(21)-C(22)	1.385(8)	C(6)-S(1)	1.755(3)
C(6)-C(7)	1.430(6)	C(22)-C(23)	1.361(8)	C(7)-C(8)	1.390(4)
C(7)-C(8)	1.357(6)	C(23)-C(24)	1.394(7)	C(7)-C(12)	1.395(4)
C(7)-C(12)	1.507(6)	C(24)-C(25)	1.431(6)	C(7)-N(1)	1.418(3)
C(8)-N(1)	1.435(5)	C(25)-C(26)	1.350(6)	C(8)-C(9)	1.383(5)
C(8)-C(9)	1.478(6)	C(25)-C(30)	1.503(6)	C(9)-C(10)	1.389(5)
C(9)-O(3)	1.460(5)	C(26)-N(2)	1.427(6)	C(10)-C(11)	1.377(5)
C(10)-O(4)	1.195(5)	C(26)-C(27)	1.478(6)	C(11)-C(12)	1.393(4)
C(10)-O(3)	1.338(5)	C(27)-O(7)	1.458(6)	C(12)-C(13)	1.446(4)
C(10)-C(11)	1.483(7)	C(28)-O(8)	1.174(7)	C(13)-C(14)	1.357(4)
C(13)-C(14)	1.382(6)	C(28)-O(7)	1.272(6)	C(13)-C(15)	1.469(4)
C(13)-C(18)	1.385(5)	C(28)-C(29)	1.446(8)	C(14)-N(1)	1.387(3)
C(13)-S(1)	1.754(4)	C(31)-C(36)	1.384(6)	C(15)-O(3)	1.217(3)
C(14)-C(15)	1.376(7)	C(31)-C(32)	1.385(6)	C(15)-C(16)	1.498(4)
C(15)-C(16)	1.370(7)	C(31)-S(2)	1.754(4)	C(16)-C(17)	1.502(4)
C(32)-C(33)	1.391(7)	N(1)-S(1)	1.662(3)	N(1)-S(1)	1.668(2)
C(33)-C(34)	1.360(7)	N(2)-S(2)	1.666(4)	O(1)-S(1)	1.425(2)
C(34)-C(35)	1.374(7)	O(1)-S(1)	1.421(3)	O(2)-S(1)	1.426(2)
C(35)-C(36)	1.379(7)	O(2)-S(1)	1.427(3)		
O(6)-S(2)	1.425(4)	O(5)-S(2)	1.423(4)		

Table 3: Selected bond angles [°] for Compounds

COMPOUND 1				COMPOUND 2			
Bond	Bond Angle [°]	Bond	Bond Angle [°]	Bond	Bond Angle [°]	Bond	Bond Angle [°]
C(2)-C(1)-C(6)	121.4(4)	C(15)-C(14)-C(13)	119.4(4)	C(1)-C(2)	119.0(3)	C(10)-C(9)-H(9)	119
C(2)-C(1)-N(1)	131.2(4)	C(15)-C(14)-H(14)	120.3	C(6)-C(1)-H(1)	120.5	C(11)-C(10)-C(9)	121.0(3)
C(3)-C(2)-C(1)	117.3(5)	C(13)-C(14)-H(14)	120.3	C(2)-C(1)-H(1)	120.5	C(11)-C(10)-H(10)	119.5
C(3)-C(2)-H(2)	121.4	C(16)-C(15)-C(14)	120.0(5)	C(3)-C(2)-C(1)	120.8(3)	C(9)-C(10)-H(10)	119.5
C(1)-C(2)-H(2)	121.4	C(16)-C(15)-H(15)	120	C(3)-C(2)-H(2)	119.6	C(10)-C(11)-C(12)	118.7(3)
C(2)-C(3)-C(4)	122.2(5)	C(14)-C(15)-H(15)	120	C(1)-C(2)-H(2)	119.6	C(10)-C(11)-H(11)	120.6
C(2)-C(3)-H(3)	118.9	C(17)-C(16)-C(15)	120.6(5)	C(2)-C(3)-C(4)	119.7(3)	C(12)-C(11)-H(11)	120.6
C(4)-C(3)-H(3)	118.9	C(17)-C(16)-H(16)	119.7	C(2)-C(3)-H(3)	120.1	C(11)-C(12)-C(7)	118.9(3)
C(5)-C(4)-C(3)	120.3(5)	C(15)-C(16)-H(16)	119.7	C(4)-C(3)-H(3)	120.1	C(14)-C(13)-C(15)	125.9(3)
C(5)-C(4)-H(4)	119.9	C(16)-C(17)-C(18)	120.7(5)	C(3)-C(4)-C(5)	120.6(3)	C(12)-C(13)-C(15)	127.2(2)
C(3)-C(4)-H(4)	119.9	C(16)-C(17)-H(17)	119.7	C(3)-C(4)-H(4)	119.7	C(13)-C(14)-H(14)	125

C(4)-C(5)-C(6)	119.2(5)	C(18)-C(17)-H(17)	119.7	C(5)-C(4)-H(4)	119.7	N(1)-C(14)-H(14)	125
C(4)-C(5)-H(5)	120.4	C(17)-C(18)-C(13)	118.7(4)	C(6)-C(5)-C(4)	119.0(3)	O(3)-C(15)-C(13)	120.7(3)
C(6)-C(5)-H(5)	120.4	C(17)-C(18)-H(18)	120.7	C(6)-C(5)-H(5)	120.5	O(3)-C(15)-C(16)	121.9(3)
C(5)-C(6)-C(1)	119.5(4)	C(13)-C(18)-H(18)	120.7	C(4)-C(5)-H(5)	120.5	C(13)-C(15)-C(16)	117.5(2)
C(5)-C(6)-C(7)	132.2(5)	C(20)-C(19)-C(24)	120.3(5)	C(5)-C(6)-C(1)	120.8(3)	C(15)-C(16)-C(17)	115.4(3)
C(8)-C(7)-C(12)	127.8(4)	C(20)-C(19)-N(2)	132.2(5)	C(5)-C(6)-S(1)	119.7(2)	C(14)-N(1)-S(1)	121.48(19)
C(6)-C(7)-C(12)	123.7(4)	C(21)-C(20)-C(19)	117.8(5)	C(1)-C(6)-S(1)	119.5(2)	C(7)-N(1)-S(1)	127.82(18)
C(7)-C(8)-C(9)	127.6(4)	C(21)-C(20)-H(20)	121.1	C(8)-C(7)-C(12)	123.2(3)	O(1)-S(1)-O(2)	121.17(13)

Table 4: Selected Torsion angles [Å] for Compounds

COMPOUND 1		COMPOUND 2			
BOND	TORSION ANGLE [°]	BOND	TORSION ANGLE [°]	BOND	TORSION ANGLE [°]
N(1)-C(1)-C(2)-C(3)	179.4(4)	S(2)-C(31)-C(36)-C(35)	-178.0(4)	C(4)-C(5)-C(6)-S(1)	179.9(3)
C(4)-C(5)-C(6)-C(7)	179.8(5)	C(2)-C(1)-N(1)-C(8)	-180.0(4)	C(2)-C(1)-C(6)-S(1)	179.7(2)
N(1)-C(1)-C(6)-C(5)	179.2(4)	C(6)-C(1)-N(1)-S(1)	-170.1(3)	N(1)-C(7)-C(8)-C(9)	-178.4(3)
C(2)-C(1)-C(6)-C(7)	179.3(4)	C(9)-C(8)-N(1)-C(1)	-177.8(4)	C(10)-C(11)-C(12)-C(13)	179.5(3)
C(5)-C(6)-C(7)-C(8)	-177.9(5)	C(7)-C(8)-N(1)-S(1)	170.2(3)	N(1)-C(7)-C(12)-C(11)	179.2(2)
C(1)-C(6)-C(7)-C(12)	-178.1(4)	C(20)-C(19)-N(2)-C(26)	179.3(5)	C(8)-C(7)-C(12)-C(13)	-178.8(2)
C(12)-C(7)-C(8)-N(1)	177.1(4)	C(24)-C(19)-N(2)-S(2)	-168.0(3)	C(11)-C(12)-C(13)-C(14)	179.4(3)
C(6)-C(7)-C(8)-C(9)	178.1(4)	C(27)-C(26)-N(2)-C(19)	-179.6(4)	C(7)-C(12)-C(13)-C(15)	179.9(2)
S(1)-C(13)-C(14)-C(15)	176.1(4)	C(25)-C(26)-N(2)-S(2)	167.3(3)	C(15)-C(13)-C(14)-N(1)	-178.6(2)
S(1)-C(13)-C(18)-C(17)	-175.6(4)	C(11)-C(10)-O(3)-C(9)	-175.5(4)	C(14)-C(13)-C(15)-O(3)	179.4(3)
N(2)-C(19)-C(20)-C(21)	178.5(4)	C(8)-C(9)-O(3)-C(10)	-174.2(4)	C(12)-C(13)-C(15)-C(16)	178.5(3)
C(22)-C(23)-C(24)-C(25)	179.6(5)	C(29)-C(28)-O(7)-C(27)	175.0(5)	C(13)-C(15)-C(16)-C(17)	-168.7(3)
N(2)-C(19)-C(24)-C(23)	-179.9(4)	C(26)-C(27)-O(7)-C(28)	163.9(5)	C(13)-C(14)-N(1)-S(1)	-166.00(18)
C(20)-C(19)-C(24)-C(25)	-179.8(4)	C(1)-N(1)-S(1)-O(1)	-157.7(3)	C(8)-C(7)-N(1)-C(14)	179.7(3)
C(23)-C(24)-C(25)-C(26)	-178.6(5)	C(8)-N(1)-S(1)-O(2)	165.0(3)	C(12)-C(7)-N(1)-S(1)	164.18(19)
C(19)-C(24)-C(25)-C(30)	-179.7(4)	C(18)-C(13)-S(1)-O(1)	174.6(3)	C(14)-N(1)-S(1)-O(1)	-163.8(2)
C(30)-C(25)-C(26)-N(2)	178.4(4)	C(36)-C(31)-S(2)-O(5)	174.0(4)	C(7)-N(1)-S(1)-O(2)	165.4(2)
C(24)-C(25)-C(26)-C(27)	-179.5(4)	C(32)-C(31)-S(2)-O(6)	-137.1(4)	C(5)-C(6)-S(1)-O(1)	149.7(3)
S(2)-C(31)-C(32)-C(33)	178.4(4)			C(1)-C(6)-S(1)-O(2)	-166.0(2)

Table 5: Hydrogen bonds for the Compound 1 [Å]

D-H...A	d(D-H)	H...A	D...A	D—H...A
C(2)-H(2)...O(2)	0.93	2.3	2.886(6)	120.3
C(9)-H(9B)...O(1)	0.97	2.25	2.908(6)	123.9
C(20)-H(20)...O(6)	0.93	2.33	2.906(7)	119.9
C(27)-H(27B)...O(5)	0.97	2.33	2.899(7)	116.9
C(29)-H(29B)...O(4)#1	0.96	2.65	3.452(7)	141.4
C(29)-H(29C)...O(4)	0.96	2.66	3.405(6)	135.1

Symmetry transformations : #1 -x+2, -y+1, -z+1

Table 6: Hydrogen bonds for the Compound 2 [Å]

D-H...A	d(D-H)	H...A	D...A	D—H...A
C(1)-H(1)...O(3)#1	0.93	2.56	3.194(4)	126.1
C(8)-H(8)...O(1)	0.93	2.46	3.028(4)	119.4
C(14)-H(14)...O(1)#2	0.93	2.54	3.412(3)	156.1

Symmetry transformations : #1 x+1/2, -y+3/2, -z+1 #2 x-1/2, y, -z+3/2

3.2. Hirshfeld surface analysis

Fig. 5-8 shows the d_{norm} , curvature, shape index, and fragment patches of indole derivatives. In the d_{norm} , the sum of vdw radii is denoted by the presence of a white color and blue color shows the short contact distances from the vdw radii. In the curvature, we can see the presence of green and blue colors which show the stacking of the molecules in the crystal. The fingerprint plots are shown in Fig. 9-12 and indicate the contribution of different type of intermolecular interactions of the molecule in the crystal. The bright-red spots on the Hirshfeld surface mapped over d_{norm} , show the presence of C-H-O interactions with neighbouring molecules. The large flat region, shows on the curvature map, and confirms the presence of C-H-O interactions in compound 2.

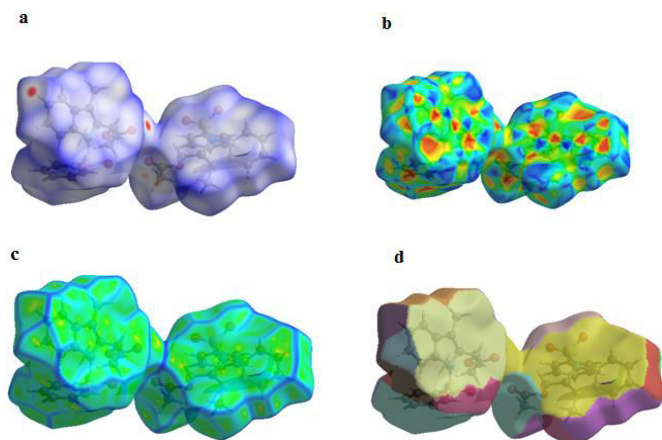


Fig. 5: View of the Hirshfeld surface mapped over a) d_{norm} b) shape index c) curvature d) fragment patches for compound 1.

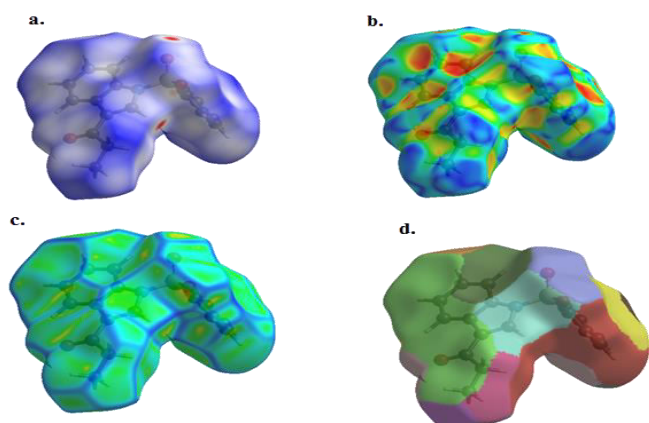


Fig. 6: View of the Hirshfeld surface mapped over a) d_{norm} b) shape index c) curvature d) fragment patches for compound 2.

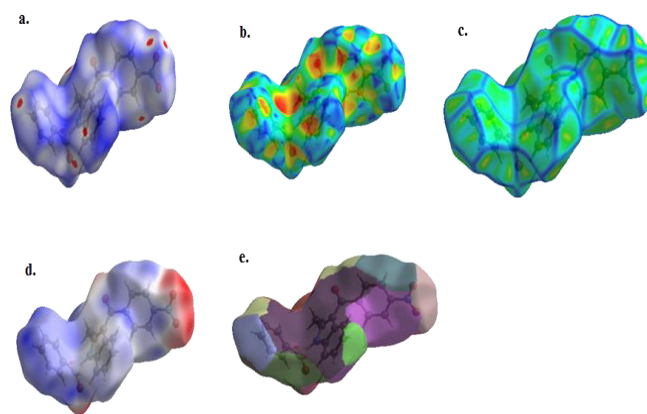


Fig. 7: View of the Hirshfeld surface mapped over a) d_{norm} b) shape index c) curvature d) fragment patches for compound 3.

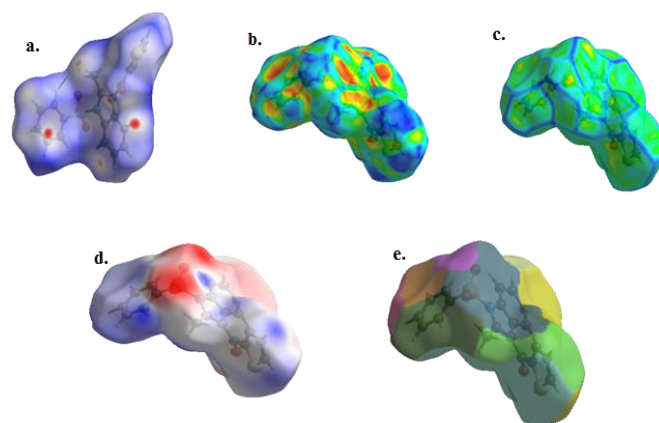


Fig. 8: View of the Hirshfeld surface mapped over a) d_{norm} b) shape index c) curvature d) fragment patches for compound 4.

The fragment patches on the Hirshfeld surface show the coordination environments of the molecules. The H-H interactions make the largest contributions to the overall Hirshfeld surfaces [46.1% for compound 1, 40.6% for compound 2, 33.3% for compound 3 and 33.4% for compound 4]. The C-H interactions appear as two wings in the fingerprint plot, showing a contribution of 18.9% for compound 1, 29.3% for compound 2, 20.2% for compound 3 and 26.9% for compound 4 of the Hirshfeld surfaces.

3.3. Molecular Docking studies

Several literature citations indicate that indole based derivatives are show biological activity of anti-tumor and anticancer activity [64-65]. Based on a literature survey, anti-cancer drug target proteins, epidermal growth factor receptors and p38 alpha MAP kinase have

been chosen for molecular docking and carried out for these four compounds. To understand the binding affinity of synthesized compounds against cancer drugs, a target protein was studied. From the EGFR docking results, compound 1 interacts with Met793 at a distance

of 3.03Å, with a docking score of -8.38 and glide energy -39.49 kcal/mol. Compound 2 binds with the active sites of Thr854 and Lys745 at a distance of 2.84Å and 2.95Å, respectively, with the docking score of -6.98 and a glide energy of -38.65 kcal/mol.

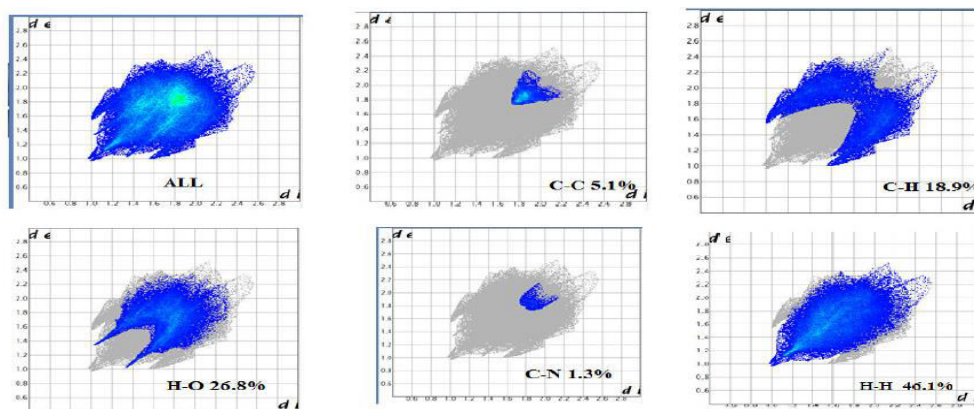


Fig. 9: The two-dimensional fingerprint plots for (a) all interactions, (b) C...C, (c) C...H, (d) H...O (e) C...N and (f) H...H interactions for compound 1.

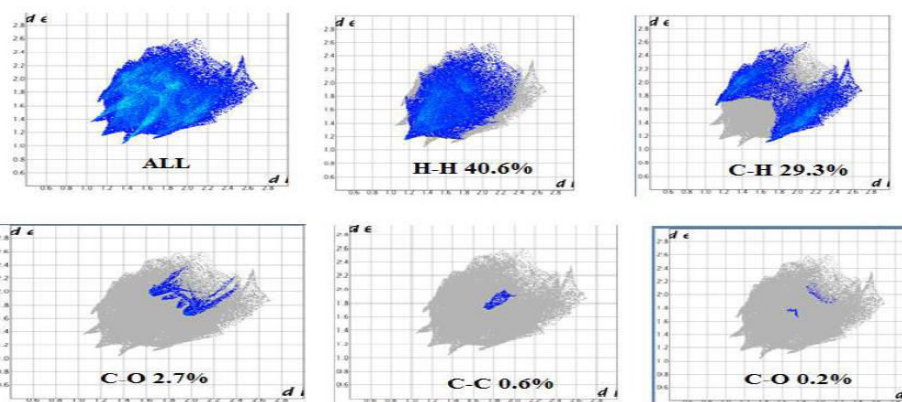


Fig. 10: The two-dimensional fingerprint plots for (a) all interactions, (b) H...H, (c) C...H, (d) C...O (e) C...C and (f) C...O interactions for compound 2.

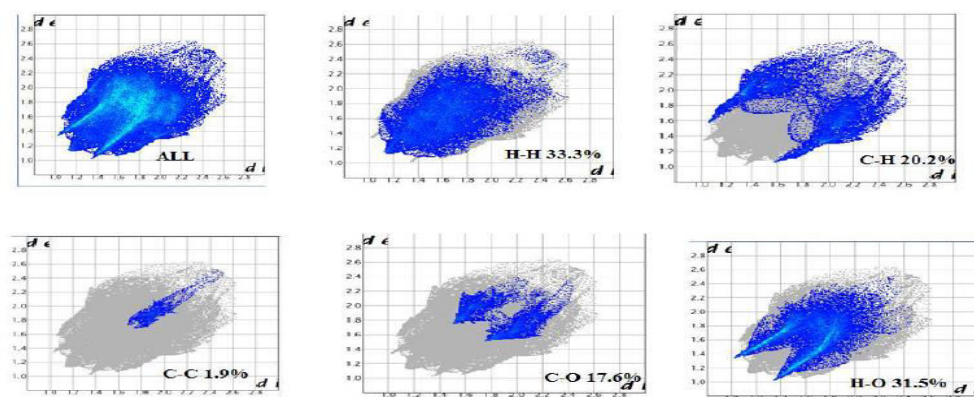


Fig. 11: The two-dimensional fingerprint plots for (a) all interactions, (b) H...H, (c) C...H, (d) C...O (e) C...C and (f) C...O interactions for compound 3.

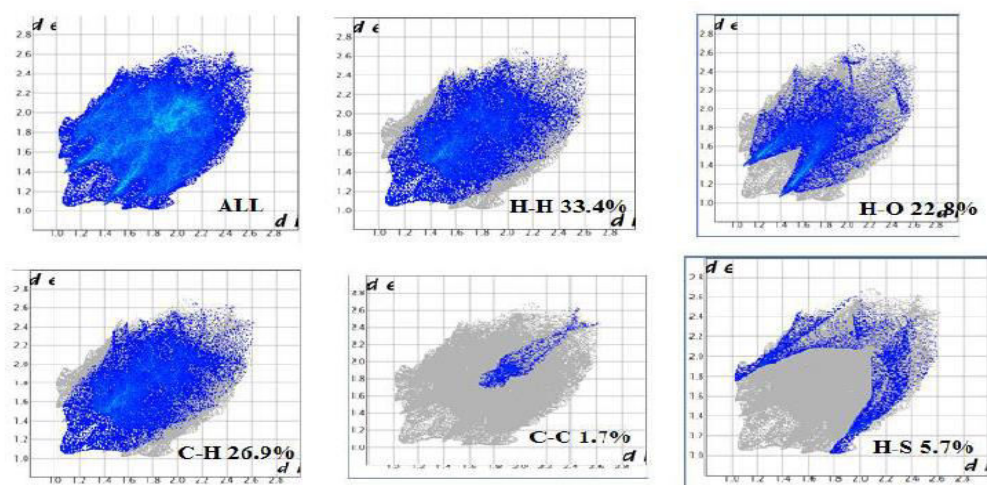


Fig. 12: The two-dimensional fingerprint plots for (a) all interactions, (b) H...H, (c) C...H, (d) C...O (e) C...C and (f) C...O interactions for compound 4.

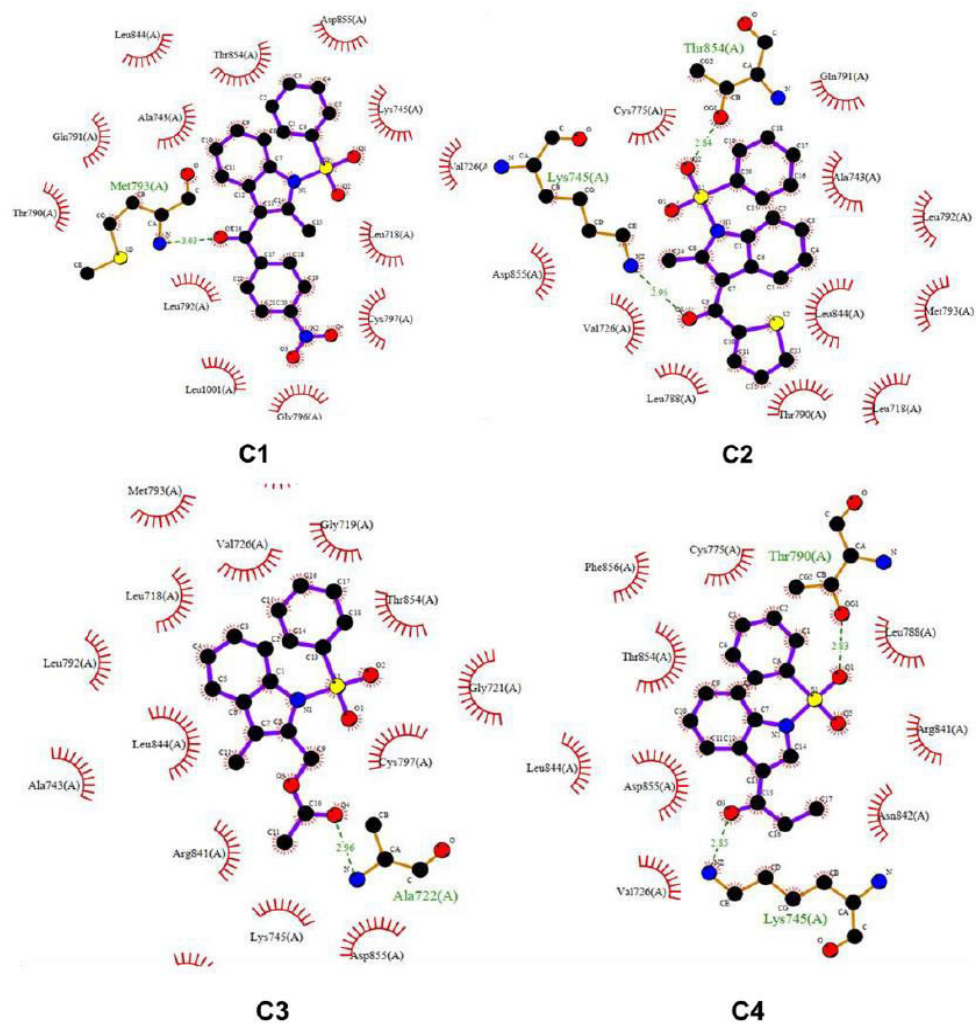


Fig. 13: Ligand interaction of synthesized compounds against the anti-cancer target, EGFR protein (Ligplot view)

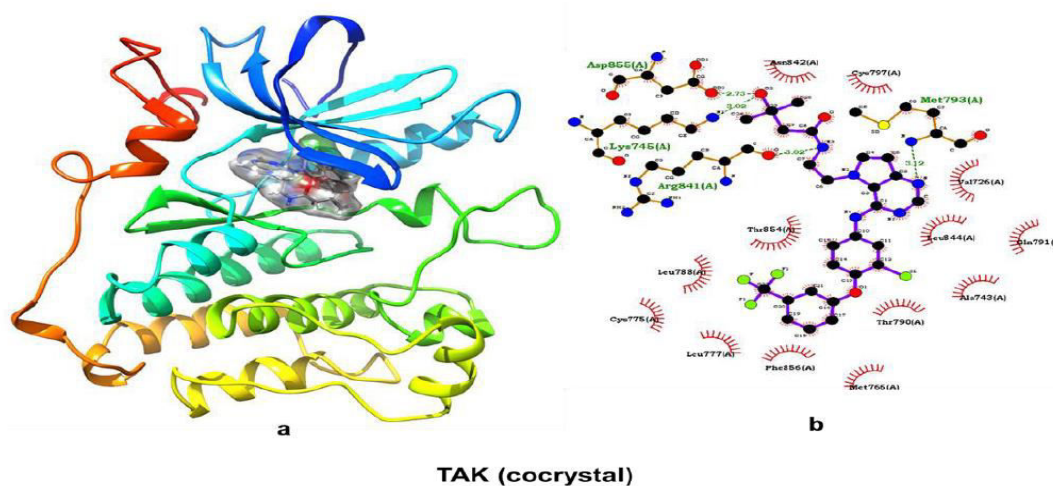


Fig. 14: Ligand interaction of native cocystal inhibitors against the anti-cancer target EGFR protein (a) Cartoon representation (b) Ligplot view.

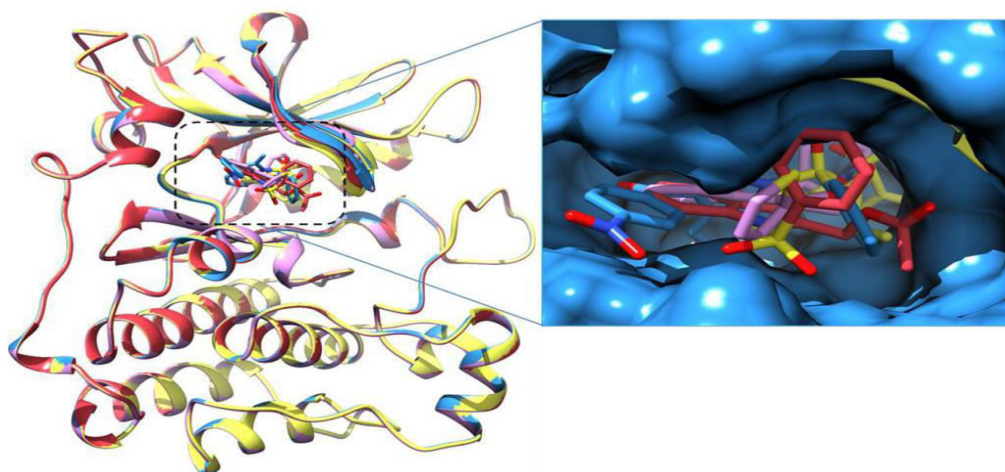


Fig. 15: Superposition of all synthesized compounds docked conformation at the active sites of EGFR.

Similarly, compounds 3 and 4 also bind with active sites of Ala722, Thr790 and Lys745 at a distance of 2.96Å, 2.83Å and 2.85Å, respectively, with a docking score of -7.03, -9.48 and a glide energy of -52.96 & -50.51 kcal/mol. To compare the binding affinity of an active cocystal the compounds were docked with the epidermal growth factor receptor at the active site. Cocystal native inhibitor (TAK) showed a docking score of -14.83 and glide energy of -81.41, and it has hydrogen bond interaction with Asp855, Arg841, Met793 and Lys745. All the synthesized compounds bind with catalytic sites similar to the cocystal compound. Interestingly compounds 1, 2 and 4 are have common hydrogen bond interactions with the active sites of Lys745 and the same hydrogen bond can be found to be a cocystal inhibitor.

IFD results were tabulated in Table 7 and ligand interactions of the compounds and cocystal are shown in Figure 13 and Figure 14. Figure 15 depicts a superposition of all of the docked complexes of the compounds, and emphasizes that all of the compounds bind with active sites of the cancer target EGFR protein. In addition, we have also taken p38 alpha MAP kinase cancer target for docking studies which plays an important role in the coordination of the cellular responses to many stress stimuli and p38 alpha involved with several upstream MAP3K's, with apoptosis signal regulating kinase. The four synthesized compounds were docked in top38 alpha, and all of the compounds have hydrogen bond interaction with catalytic sites of Met109, Lys35, Phe169, Asp168 and Ala51.

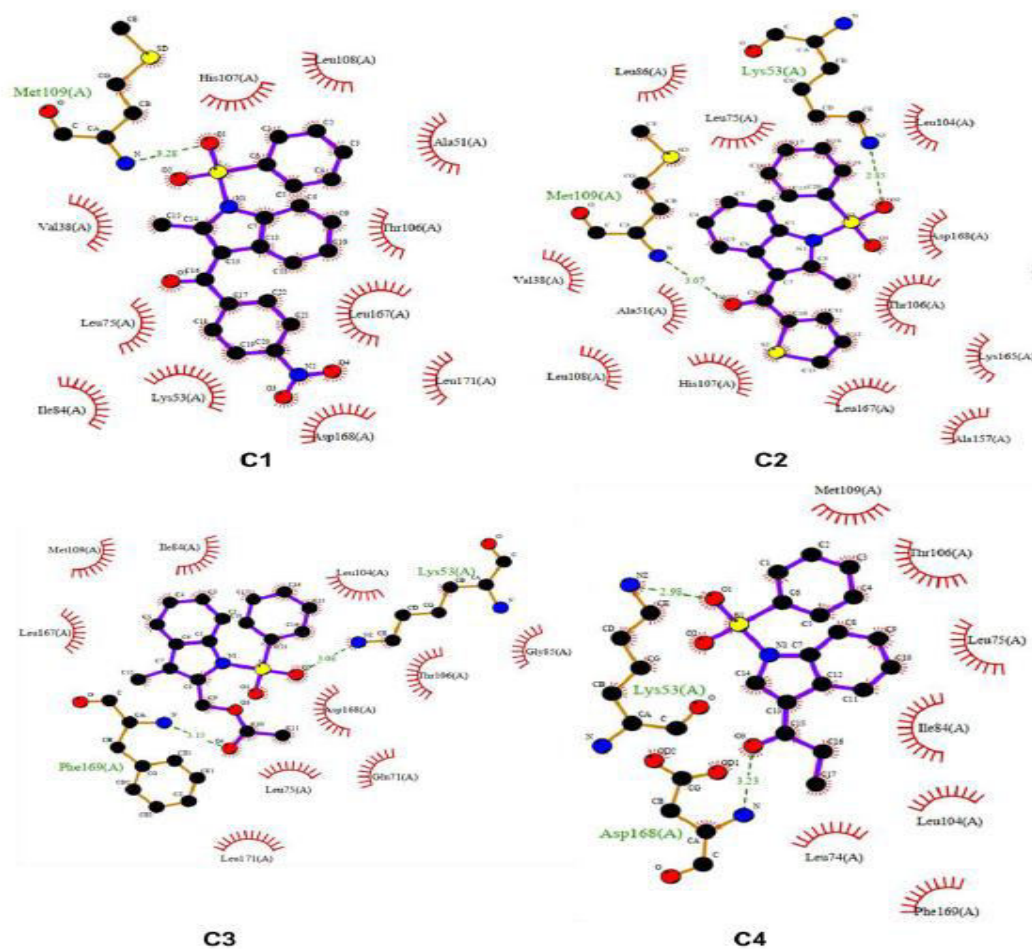


Fig. 16: Ligand interaction of native cocystal inhibitors against the anti-cancer target p38 MAP kinase (a) Cartoon representation (b) Ligplot view

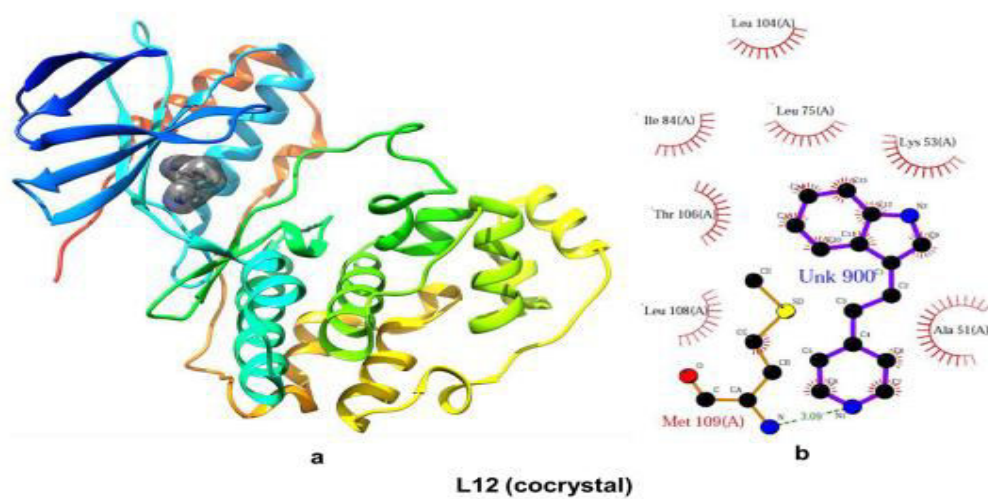


Fig.17: Ligand interaction of native cocystal inhibitors against the anti-cancer target p38 MAP kinase (a) Cartoon representation (b) Ligplot view

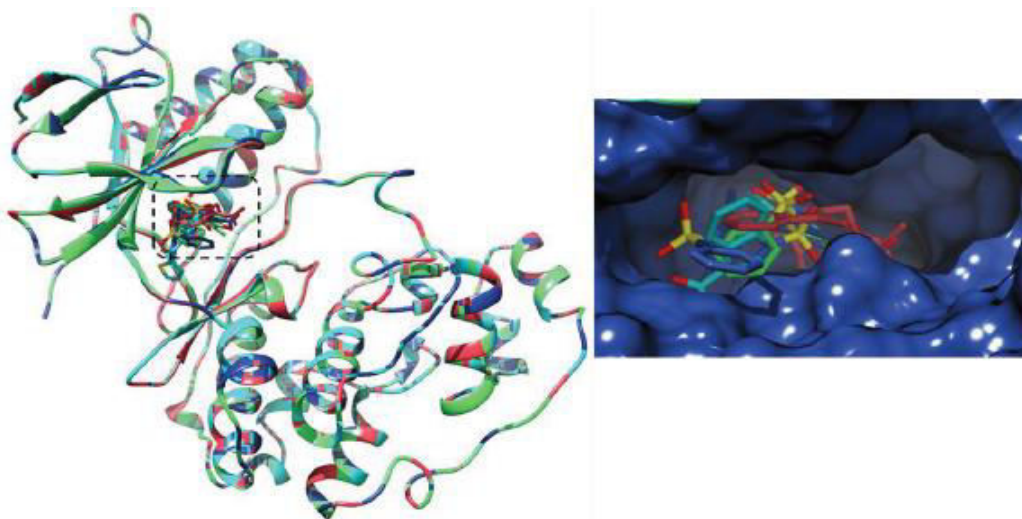


Fig.18: Superposition of all synthesized compounds docked conformation at the active sites.

Table 7: Docking score and Glide energy of Crystal compounds docked with EGFR.

Compounds	Docking score (kcal/mol)	Glide energy (kcal/mol)	Hydrogen Bond Interactions (D-H...A)	Distance (Å)
(C1)	-8.38	-39.49	MET793 (N-H...O)	3.03
(C2)	-6.98	-38.65	THR854 (O-H...O) LYS745 (N-H...O)	2.84 2.95
(C3)	-7.03	-52.96	ALA 722 (N-H...O)	2.96
(C4)	-9.48	-50.51	THR790 (O-H...O) LYS 745 (N-H...O)	2.83 2.85
Cocrystal (TAK)	-14.83	-81.41	ASP855 (O-H...O) ARG841 (N-H...O) MET793 (N-H...N) LYS745 (N-H...O)	2.73 3.02 3.12 3.02

Table 8: Docking score and Glide energy of Crystal compounds docked with P38 MAP/Alpha. ** Active sites amino acids are highlighted in bold text

Compounds	Docking score (kcal/mol)	Glide energy (kcal/mol)	Hydrogen Bond Interactions (D-H...A)	Distance (Å)
(C1)	-7.80	-46.95	MET109 (N-H...O)	3.28
(C2)	-8.45	-44.08	MET109 (N-H...O) LYS 53 (N-H...O)	3.07 2.85
(C3)	-8.40	-38.30	PHE169 (N-H...O) LYS53 (N-H...O)	3.15 3.08
(C4)	-9.15	-53.09	ASP168 (N-H...O) LYS53 (N-H...O)	3.23 2.98
L12 (Cocrystal)	-7.99	-36.25	N-H...O (ALA 51) (MET 109) N-H...O	3.01 3.14

** Active sites amino acids are highlighted in bold text

In the co-crystal a native inhibitor has same hydrogen bond with Met109 similar to and all of the compounds. The IFD result shows that the cocrystal inhibitor has a docking score of -7.99 and glide energy of -36.25, respectively. IFD results of the four synthesized

compounds indicate docking scores of -7.80, -8.45, -8.40, -9.15 and glide energies of 46.95, -44.08, -38.30, -53.09 kcal/mol. Docking results reveal that all of the compounds show better binding affinity (docking score as well as glide energy) compared with cocrystal (L12)

native inhibitor against p38 alpha map kinase target protein. Docking parameters and hydrogen bond distances are tabulated in Table: 8. The Ligand interaction profile of the docked compounds and cocrystal inhibitor are shown in Figure 16. Figure 17 represents a cartoon model of cocrystal binding with respect to the target protein, and cocrystal which are highlighted in the surfacemodel. To confirm the mode of the binding at the catalytic sites of target protein, all four docked complexes are superimposed. Figure 18 shows that all are binding at the active sites.

From above these molecular docking results suggest that all four compounds are having better binding affinity with respect to the anti-cancer targets. It reveals that this indole derivative has anti-cancer properties.

3.4. Molecular Dynamics simulation (MDS)

The tyrosine kinase EGFR and p38-MAP kinase alpha docked complexes of compound C3, C4 and TAK, L12 (Cocrystal native inhibitors) was subjected 10 ns MD simulation. To understand the dynamic behavior of the protein, structural properties were analyzed through RMSD and the C α -atom of the overall protein. The protein active sites fluctuations were observed via RMSF plots, and from the overall MD simulation time

variation in the ligand interaction of the active sites. Residues in the cavity were also observed through interaction histograms and protein–ligand contact graphs.

The target protein EGFR docked complexes, MD simulation of compound C3 from 0 ns time scale until 5ns show higher RMSD deviations up to 2.7 Å, afterwards it has slowly gotten converged until 10ns toward the end of the simulation and it shows lesser RMSD value of 1.5Å. Compound C3 shows that in the overall entire simulation (0-10 ns) time scale there is no higher deviation and its RMSD values were observed up to (0.8-1.6 Å). Comparatively, the EGFR protein cocrystal on active inhibitor (TAK) shows a convergence RMSD value of 0.8Å (Figure 19). Root mean square fluctuation (MSFs) provide residual atoms in structural flexibility of upon ligand binding in the overall protein structure. All three docked complexes, EGFR were calculated from side chain rmsf values from the figure 20. From figures 21 and 22, throughout the 10 ns time period of MD simulation trajectory, different types of protein ligand interactions were monitored and specific hydrogen and hydrophobic interactions were also observed for compounds 3, 4 and cocrystal native inhibitor.

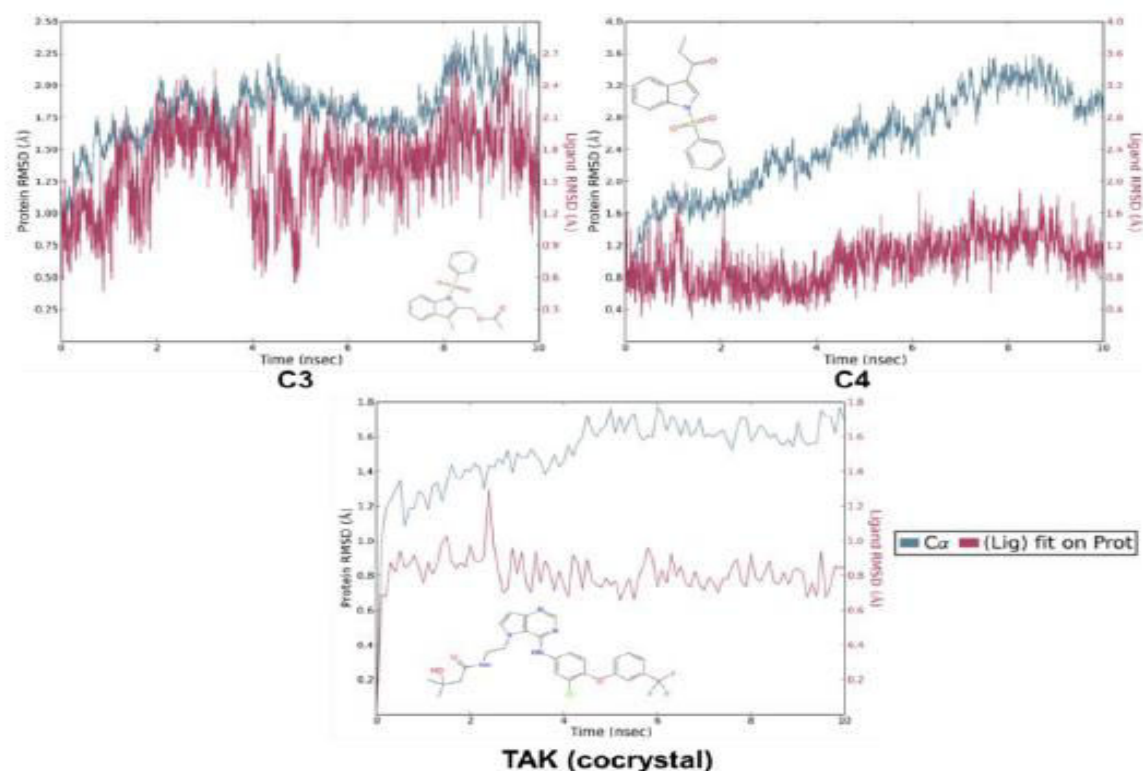


Fig. 19: RMSD plots of docked complexes of EGFR during the MD simulation.

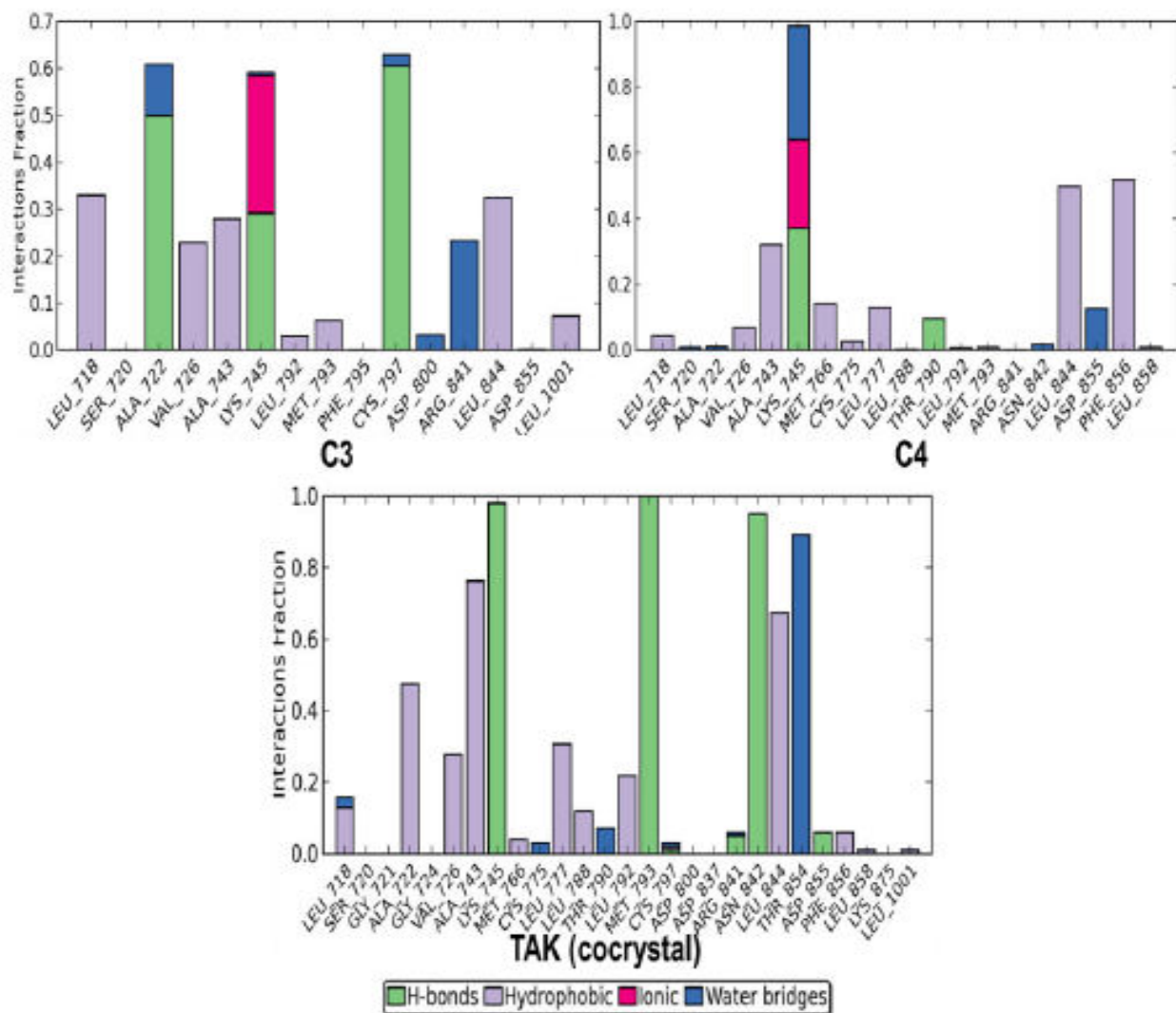


Fig.22: 2D ligand interactions of during the MD simulation for EGFR docked complexes.

Hydrogen bond interactions are more important for specific binding affinity of the protein ligand interactions. Compound 3 has a direct hydrogen bond interaction with the Ala722, Lys745 and Cys797 catalytic residues of EGFR. Compound 4 also has two Hbond interactions with Lys745 and Thr790, in the case of cocystal compound has Lys745, Met793, Arg841, Asn842 and Asp855. Water mediated interactions are also observed from all three docked complexes during the MD simulations involving Ala722, Asp800, Arg841, Lys745, Thr790 and Thr854. Several hydrophobic interactions were also found such as with Leu718, Val726, Ala743, Leu844, Phe856, Ala743 and Leu792. 2D. Ligand interactions are shown in figure 22. Similarly, another target of P38 MAP kinase alpha protein with compound 3, 4 and cocystal inhibitor MD simulations were carried out with a time period of 10

ns. To understand the structural stability of a protein ligand complex, the RMSD is an important quantitative parameter of MD simulation. During the MD run compound 3 shows stable conformations and its RMSD value 2.4 Å. Compound4 showed little deviations compared to compound 3 and RMSD value of 3.0Å. Finally, in case of the cocystal, the native inhibitor shows higher RMSD deviations and in indicates that its depict that overall complex structure has a less stable conformation with an RMSD value between 1.0 Å - 3.5Å. In the case of RMSD, compounds 3 and 4 show lesser deviations compared to cocystal native inhibitor (Figure 23). RMSFs of all three complexes were calculated during the MD simulations, with compounds 3 and 4 it showing overall residual fluctuations are much lower as it reaches a maximum below 3.0Å. The cocystal compound was also observed with a similar

RMSF value (Fig. 24). To find the major contributions in protein residues and ligands, protein-ligand interactions analysis was calculated throughout the MD simulation. Various types of interactions are observed during the MD simulation, including ionic, water mediated, Hbond and Hydrophobic interactions. Compounds 3 and 4 they have Hydrogen bond interactions with Lys45, Phe165 and Asp168 catalytic residues. In case of cocrystal (L12) only observed one Hbond with Asp168. In addition, several hydrophobic

interactions also perceived such as Leu75, Ile84, Met109, Leu167, Leu171, Ala51, Ile84, Leu104, Ala157, Lys53, Val38, Arg67, Glu71, Leu74, and Leu75 (Figure: 25). 2D Ligand interactions were shown in figure 26). From the above of the MD simulation studies of both EGFR and P38 MAP kinase anti-cancerous drug target protein docked complexes of compound 3 and compound 4 have good stability and binding properties (Hbond and Hydrophobic) similar to cocrystal native inhibitors.

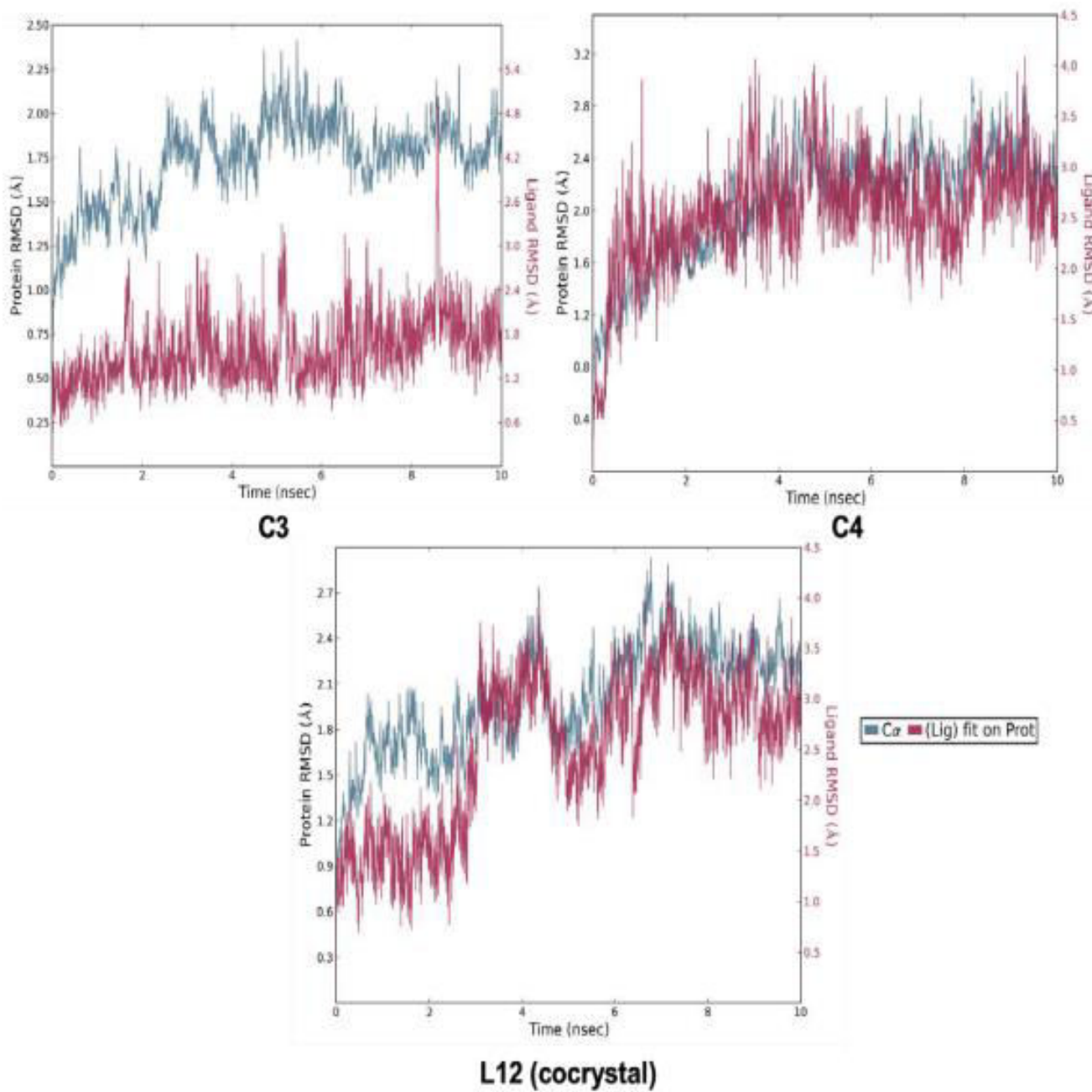


Fig. 23: RMSD plots of docked complexes of P38/MAP kinase during the MD simulation

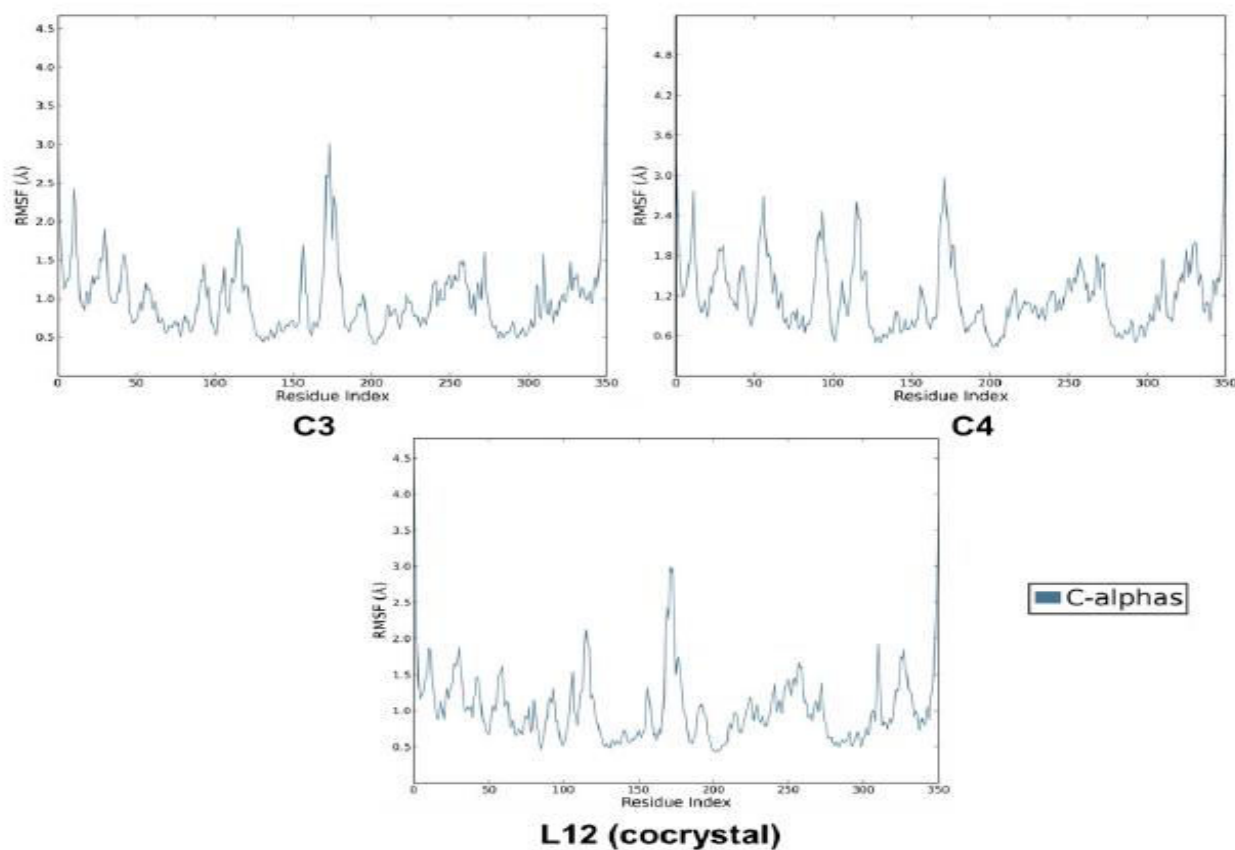


Fig. 24: RMSF plots of docked complexes of P38/MAP kinase during the MD simulation.

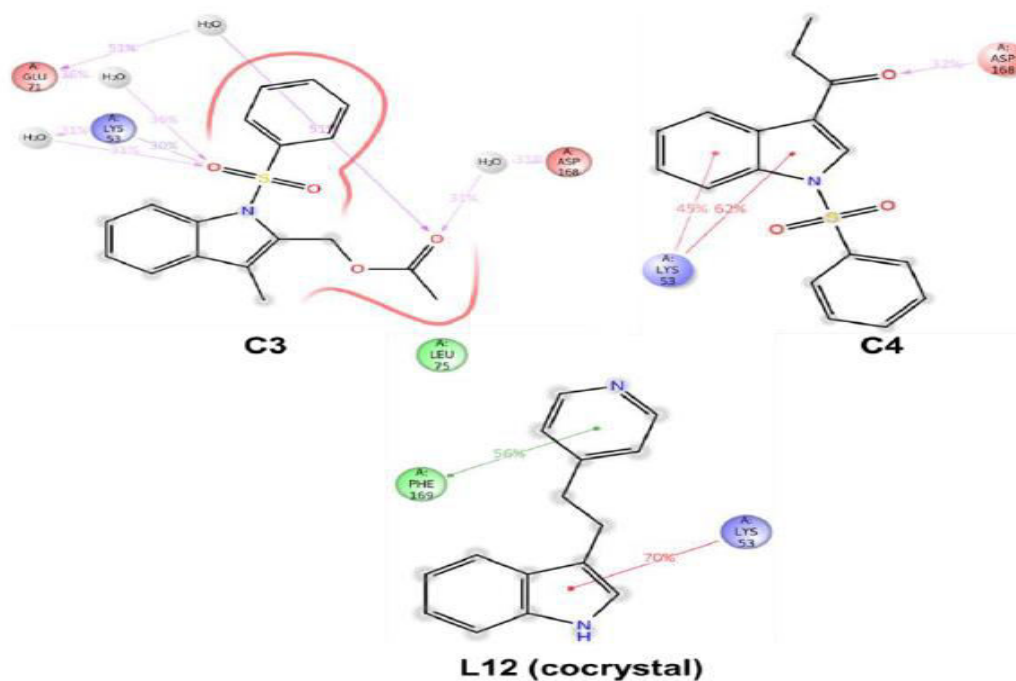


Fig 25: Hydrogen and Hydrophobic interactions of P38/MAP kinase docked complex from MD simulation.

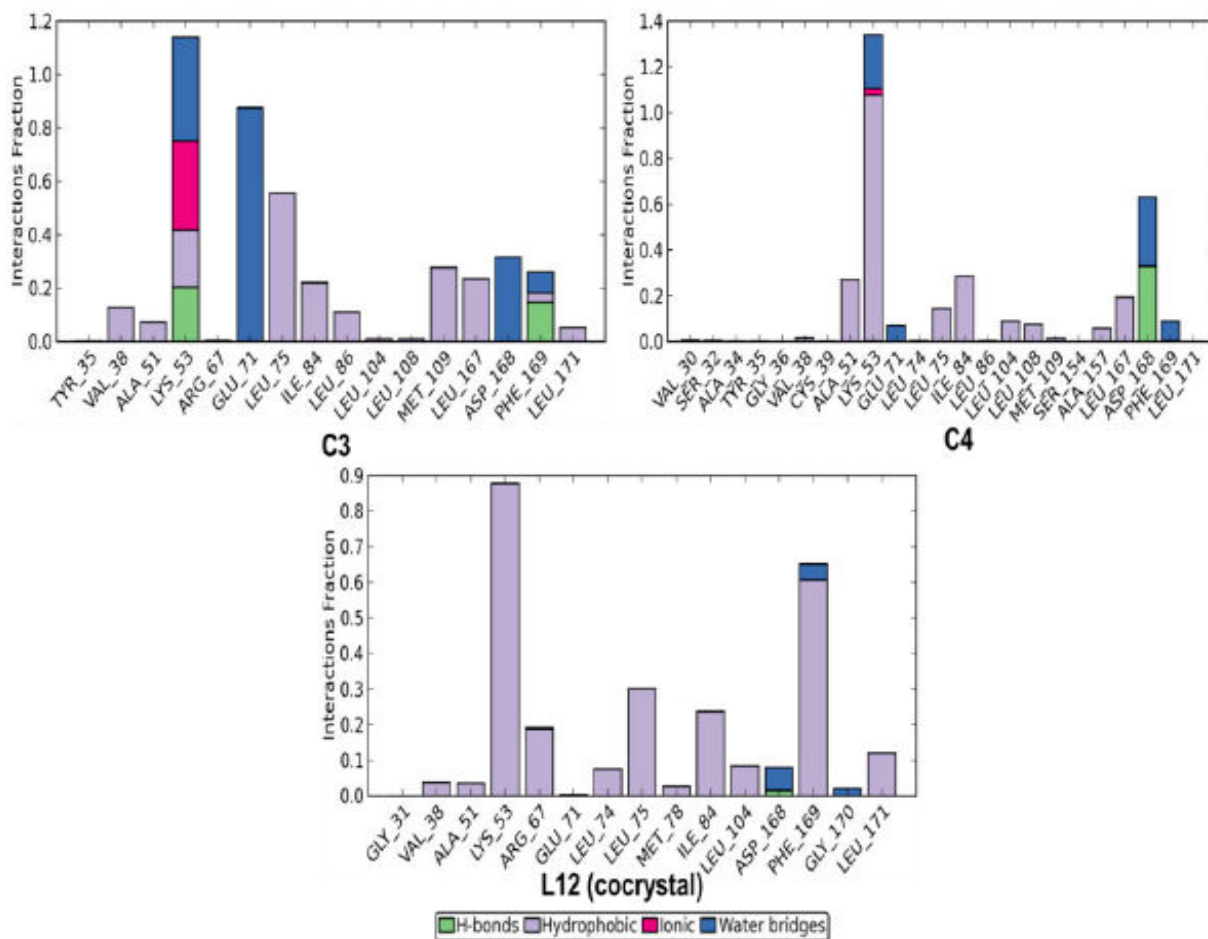


Fig 26: 2D ligand interactions of P38/ MAP kinase during the MD simulation for docked complexes.

4. CONCLUSION

The compounds were synthesized according to schemes 1 and 2. The XRD studies on the compound showed that in both compounds atom S1 has a distorted tetrahedral configuration differing from the ideal tetrahedral values attributing to the Thorpe–Ingold effect. As a result of the electron withdrawing character of the phenylsulfonyl group, in both compounds the N–C bond lengths are longer than the mean value of 1.355(14) Å. The geometrical results of the compounds are in good agreement with the X-ray crystallographic data and Hirshfeld surface analysis. The intermolecular contacts obtained by Hirshfeld analysis substantiate the XRD results. Based on docking results all of the compounds show better binding affinity with anti-cancer target proteins. The four compounds were employed with molecular docking studies against anti-cancer target proteins, epidermal growth factor receptor and p38 alpha MAP kinase. All of the

compounds show better binding affinity and similar to known existing cancer inhibitors. MD simulation studies suggest that both EGFR and P38 MAP kinase anti-cancerous drug target protein docked complexes of compounds 3 and 4 show good stability and binding properties (H bond and Hydrophobic) similar to cocystal native inhibitors.

5. SUPPLEMENTARY INFORMATION (SI)

Supplementary crystallographic data were deposited in CCDC (Cambridge Crystallographic Data Centre, No: 1858381, 1890533). The data can be acquired free of charge via <http://www.ccdc.cam.ac.uk/conts/retrieving.html>, or e-mail: deposit@ccdc.ac.uk.

6. ACKNOWLEDGEMENT

The authors wish to acknowledge the SAIF, IIT, Chennai for the data collection. Author DAK acknowledges the Indian Council of Medical Research for Senior Research Fellow fellowship.

7. REFERENCES

1. Sharma V, Kumar P, Pathak D. *J. Hete. Chem.*, 2010; **47(3)**:491-502.
2. Tang H, Hammack C, Ogden SC, Wen Z, Qian X, Li Y, Christian KM. *Cell stem cell.*, 2016; **8(5)**:587-590.
3. Kaushik N, Attri P, Kumar N, Kim C, Verma A, Choi E. *Mol.*, 2013; **18(6)**:6620-6662.
4. Grinev AN, Sarkisova LS, Lyubchanskaya VM, Nikolaeva IS, Golovanova EA. *Pharma.Chem.J.*, 1984; **18(9)**:618-620.
5. Singh UP, Sarma BK, Mishra PK, Ray AB. *Folia microbiologica.*, 2000; **45(2)**:173.
6. Rodriguez JG, Temprano F, Esteban Calderon C, Martinez Ripoll M, Garcia-Blanco S. *Tetrahedron*, 1985; **41(18)**:3813-3823.
7. Andreani A, Granaiola M, Leoni A, Locatelli A, Morigi R, Rambaldi M, Salvini L. *Anti-cancer drug design*, 2001; **16(2)**:167-174.
8. Porter JK, Bacon CW, Robbins JD, Himmelsbach DS, Higman HC. *J. agri food chem.*, 1977; **25(1)**:88-93.
9. Sundberg RJ. *Indoles.*, Elsevier., 1996
10. Wolf WM. *Acta Cryst. Sec.C: Cryst. Struct. Comm.*, 1999; **55(3)**:469-472.
11. Dhanalakshmi G, Ramanjaneyulu M, Thennarasu S, Aravindhan S. *Acta Cryst. Sec. E: Cryst. Comm.*, 2018; **74(12)**:1913-1918.
12. Rajeswaran WG, Labroo RB, Cohen LA, King MM. *J. Org. Chem.* 1999; **64(4)**:1369-1371.
13. Raj AA, Raghunathan R, Sridevi Kumari MR, Raman N. *Bio. & Medi. Chem.*, 2003; **11(3)**:407-419.
14. Hendi SB, Basanagoudar LD. *Ind. J.of chem. Sec. B- Org. Chem.*, 1981; **20(4)**:288-289.
15. Kolocouris N, Foscolos GB, Kolocouris A, Marakos P, Pouli N, Fytas G, DeClercq E. *J. Medi. Chem.*, 1994; **37(18)**:896-2902.
16. Stuart DR, Bertrand-Laperle M, Burgess KM, Fagnou K. *J. Ame. Chem. Soc.*, 2008; **130(49)**:16474-16475.
17. Mun HS, Ham WH, Jeong JH. *J. comb. Chem*, 2005; **7(1)**:130-135.
18. Li JJ, Gribble GW, *Palladium in Heterocyclic Chemistry: A Guide for the Synthetic Chemist*; 2000.
19. Gilchrist TL, *Chem. Soc., Perkin Transactions.*, 2001; **1(20)**:2491-2515.
20. Baran PS, Guerrero CA, Ambhaikar NB, Hafensteiner D. *Chem. Inter.Edition*, 2005; **44(4)**:606-609.
21. Nigovic B, Antolic S, Kojic-Prodic B, Kiralj, Magnus V, Salopek-Sondi B. *Acta Cryst. Sec. B; Stru. Sci.*, 2000; **56(1)**:94-111.
22. Quetin-Leclercq J. *J. de Pharm. De Belg.*, 1994; **49(3)**:181-192.
23. Grogin NA, Kocevski DD, Faber SM, Ferguson HC, Koekemoer AM, Riess AG, Barden M. *Astro. phy. J. Suppl. Series*, 2011; **197(2)**:35.
24. Kim KH, Chahine G, Franc JP, Karimi A. *Advanced experimental and numerical techniques for cavitation erosion prediction*, (Eds) 2014; **106**:springer.
25. Kaushik A, See-Think-Do A content, marketing, measurement business framework. *Occam's razor*; 2013.
26. Fernandez JA, Adolphsen C, Akay AN, Aksakal H, Albacete JL, Alekhin S, Armesto N. *J. Phy. G: Nuclear and Particle Physics*, 2013; **39(7)**:075001.
27. Sharma V, Kumar P, Pathak D. *J. Hete. Chem.*, 2010; **47(3)**:491-502.
28. Kerr JM, DePinto JV, McGrath D, Sowa SP, Swinton SM. *Journal of Great Lakes Research*, 2016; **42(6)**:1252-1259.
29. Avendaño C, Menéndez J. *Med. Chem. of anticancer agents*; 2008.
30. Gleeson M, Clarke R. *Scott-Brown's Otorhinolaryngology: Head and Neck Surgery*, Eds 2008; **7Ed (3)**: CRC Press.
31. Bridges EM, Harris AL. 2011Eds; **81(10)**:1183-1191.
32. Dhanalakshmi G, Saravanan V, Mohanakrishnan AK, Aravindhan S *Acta Cryst. Sec. E: Crystal. Comm.*, 2017; **73(10)**:555-1559.
33. Bruker A P E X, Saint and SADABS, 2009: Bruker AXS Inc, Madison, Wisconsin, USA.
34. Sheldrick GM. *Acta Crysta. Sec. C., Struc. Chem.*, 2015; **71(1)**:3-8.
35. Macrae CF, Bruno IJ, Chisholm JA, Edgington PR, McCabe P, Pidcock E, Wood PA. *J. of App. Crystal*, 2008; **41(2)**:466-470.
36. Farrugia LJ. *J. App.cryst.*, 2012; **45(4)**:849-854.
37. Spek AL. *Acta Cryst. Sec. D, Bio. Cryst.*, 2009; **65(2)**:148-155.
38. Spackman MA, Jayatilaka D. *Cryst. Eng. Comm*, 2009; **11(1)**:19-32.
39. Hirshfeld FL. *Theoretica. chimica. acta.*, 1977; **44(2)**:129-138.
40. Spackman M, McKinnon JJ. *Cryst Eng Comm.*, 2002; **4(66)**:378-392.

41. Dalal J, Sinha N, Yadav H, Kumar B. *RSC Advances*, 2015; **5(71)**:57735-57748.
42. Wolff SK, Grimwood DJ, MA Spackman, JJ McKinnon. *Cryst.Eng.Comm*, **4**; 378-392.
43. Ghalla H, Issaoui F, Bardak A *Atac. Comput. Mater. Sci.*, 2018; **149**:291.
44. McKinnon JJ, Spackman MA, Mitchell AS. *Acta Cryst. Section B: Struc. Sci*, 2004; **60(6)**:627-668.
45. Parkin A, Barr G, Dong W, Gilmore CJ, Jayatilaka D, McKinnon JJ, Wilson CC. *Cryst Eng Comm*, 2007; **9(8)**:648-652.
46. Spackman MA, McKinnon JJ, Jayatilaka D. *Cryst. Eng. Comm*, 2008; **10(4)**:377-388.
47. Spackman MA, Jayatilaka D. *Cryst. Eng. Comm*, 2009; **11(1)**:19-32.
48. Aertgeerts K, Skene R, Yano J, Sang BC, Zou H, Snell G, et al. *J Biol Chem.*, 2011; **286(21)**:18756-18765.
49. Gill AL, Frederickson M, Cleasby A, Woodhead SJ, Carr MG, Woodhead AJ, et al. *Med. Chem.*, 2005; **48(2)**:414-426.
50. Glide .2014-2 version 6.0, *Schrödinger*, LLC, New York.
51. Ligprep, 2014-2.version 2.3, *Schrödinger*, LLC, New York.
52. Brooks BR, Bruccoleri RE, Olafson BD, States D, Swaminathan S, Karplus M *Charmm. J. Comp. Chem.*, 1983; **4**:187-217.
53. Rinn William E. 2007; **13(4)**:721-722.
54. Galeazzi Roberta. *Curr. Comput Aided Drug Des*, 2009; **4**:225-240.
55. Maragakis P, Lindorff-Larsen K, Eastwood MP, Dror RO, Klepeis JL, Arkin IT, et al. *J. Phys.Chem. B*, 2008; **12(19)**:6155-6158.
56. Gupta SC, Kapoor K. *Fundamentals of applied statistics*, 2019; Sulthan Chand & Sons.
57. Iqbal S, Balasubramanian ARK, Gunasekaran K. *Amer. J. of Drug Deli. Thera.*, 2016; **3(2)**:1-12.
58. Selvakumar R, Anantha Krishnan D, Ramakrishnan C, Velmurugan D, Gunasekaran K. *J. of Bio. Strut.and Dyn.*, 2019; 1-15.
59. Umadevi M, Saravanan V, Yamuna R, Mohanakrishnan AK, Chakkaravarthi G. *Acta Crystal. Sec. E: Crystall. Comm*, 2015; **71(2)**:133-135.
60. Beddoes RL, Dalton L, Joule JA, Mills OS, Street JD, Watt CI. *Journal of the Chemical Society Perkin Transactions*, 1986; **2(6)**:787-797.
61. Kamala Kumar C, Dhayalan V, Mohanakrishnan AK, Balasubramanian V, Manivannan V *Actacystallographica Section E: Structure Reports Online.*, 2011; **67(3)**:o741.
62. Bassindale AR, Stout T. *J. organo. chem.*, 1984; **271(1-3)**:C1-C3.
63. Allen FH, Kennard O, Watson DG, Brammer L, Orpen AG, Taylor R. *Journal of the Chemical Society, Perkin Transactions.*, 1987; **2(12)**:S1-S19.
64. Goswami A, Rathi AK, Aparicio C, Tomanec O, Petr M, Pocklanova R., et al. *ACS applied materials & interfaces*, 2017; **9(3)**:2815-2824.
65. Singh Sidhu J, Singla R, Jaitak V. *Anti-Cancer Agents in Medicinal Chemistry*, 2016; **16(2)**:160-173.